



HAL
open science

Domain structure and energy losses up to 10 kHz in grain-oriented Fe-Si sheets

A. Magni, A. Sola, Olivier de La Barriere, Enzo Ferrara, Luca Martino, C. Ragusa,
C. Appino, F. Fiorillo

► To cite this version:

A. Magni, A. Sola, Olivier de La Barriere, Enzo Ferrara, Luca Martino, et al.. Domain structure and energy losses up to 10 kHz in grain-oriented Fe-Si sheets. *AIP Advances*, 2021, 11 (1), pp.015220. <10.1063/9.0000184>. <hal-03316102>

HAL Id: hal-03316102

<https://hal.science/hal-03316102v1>

Submitted on 6 Aug 2021

HAL is a multi-disciplinary open access archive for the deposit and dissemination of scientific research documents, whether they are published or not. The documents may come from teaching and research institutions in France or abroad, or from public or private research centers.

L'archive ouverte pluridisciplinaire **HAL**, est destinée au dépôt et à la diffusion de documents scientifiques de niveau recherche, publiés ou non, émanant des établissements d'enseignement et de recherche français ou étrangers, des laboratoires publics ou privés.



HAL Authorization

Domain structure and energy losses up to 10 kHz in grain-oriented Fe-Si sheets

A. Magni¹, A. Sola¹, O. de la Barrière², E. Ferrara¹, L. Martino¹, C. Ragusa³, C. Appino¹, F. Fiorillo¹

¹*Advanced Materials Metrology and Life Science Division, INRIM, Torino, Italy*

²*Lab. SATIE, CNRS-ENS, Saclay, France*

³*Energy Department, Politecnico di Torino, Torino, Italy.*

Abstract

We investigate in theory and experiment the frequency dependence of magnetic losses in Grain-Oriented 0.29 mm thick high-permeability steel sheets up to 10 kHz. Such unusually broad frequency range, while responding to increasing trends towards high-frequency regimes in applications, is conducive to a complex evolution of the magnetization process, as imposed by increasing frequencies to a non-linear high-permeability saturable material. We show that the concept of loss decomposition, supported by observations of the domain wall dynamics through Kerr experiments, is effective in the assessment of the broadband frequency dependence of the energy loss. By calculating, in particular, the instantaneous and time averaged macroscopic induction profiles across the sheet thickness through the Maxwell's diffusion equation, the classical loss component W_{class} , versus frequency f and peak polarization J_p is obtained. Instrumental to a simplified theoretical approach is the assumption of the normal magnetization curve as the magnetic constitutive equation of the material. While the hysteresis loss W_{hyst} invariably increases with frequency, the excess loss W_{exc} , the quantity directly associated with the eddy currents circulating around the moving domain walls, tends to vanish upon increasing both frequency and induction values. The Kerr experiments actually show that, while the oscillating 180° domain walls can adjust to the depth of the induction profile by bowing at low J_p values, the magnetization reversal at high inductions and frequencies occurs by inwardly motion of symmetric fronts originating at the sheet surface, according to a classical framework.

1

2 **I. Introduction**

3 Recent trends in electrical energy generation and transmission are guided by the growing role of
4 heterogeneous and distributed renewable sources. New technologies, associated with the concept of
5 “smart grids”, are therefore developed, in order to flexibly accommodate the supply and conversion of
6 energy.^{1,2} Under these circumstances, the traditional applications of the 50 – 60 Hz power transformers
7 combine with the operation of newly introduced devices, like the solid state transformers, where high
8 frequencies and electronic controls, introducing high harmonic contents, provide a novel operating
9 landscape. Consequently, the conventional paradigms underlying the investigation and development
10 of the grain-oriented (GO) Fe-Si alloys need to evolve and widen their range.³ Transformers employed
11 in power electronics operate, for example, at kHz frequencies, with high order harmonics generated by
12 Pulse Width Modulation (PWM).⁴ In rotating electrical machines, GO sheets can provide an interesting
13 alternative to the conventional non-oriented (NO) Fe-Si alloys.⁵ It is thus shown that very high speed
14 motors display better efficiency and higher working inductions when the stator core is built by suitable
15 combination of GO and NO sheets.⁶ However, the whole matter of high-frequency response of GO
16 alloys and its quantitative interpretation have not been assessed so far. The prevalent attitude to this
17 problem is one of resorting to empirical models and formulations, like the Steinmetz’s equation.⁷⁻⁹ The
18 phenomenology of energy losses at high frequencies has actually been brought to physical treatment
19 in NO sheets, taking advantage of the fine scale of the domain structure. Here, the Maxwell’s diffusion
20 equation was solved by a Finite Element Method (FEM), with the magnetic constitutive law derived
21 from a dynamic hysteresis model.¹⁰⁻¹² It is a relatively complex approach, where one assumes that the
22 statistics of the moving domain walls (dw) applies at the scale of the single finite element, which is
23 small compared to the sheet thickness. This procedure is difficult to justify in the case of GO sheets
24 and their broad domain structure.¹³ It was suggested that, where high peak polarization values are
25 involved in GO Fe-Si (near rectangular loop), a step-like (saturating) magnetic constitutive law coupled
26 to the Maxwell’s diffusion equation, to be solved numerically¹⁴ or analytically¹⁵, applies at all
27 frequencies. The envisaged magnetization process consists, in this case, of symmetric reversal fronts,
28 propagating inwards from the sheet opposite surfaces to the midplane.¹⁶ The Kerr observations show,
29 however, that this does not happen at power frequencies, where the longitudinal bar-like domain
30 structure always survives, whatever the peak polarization.

31 In this paper, we discuss the broadband ($DC \leq f \leq 10$ kHz) frequency dependence of the energy
32 losses measured in 0.29 mm thick high-permeability GO sheets subjected to sinusoidal polarization of
33 peak values J_p ranging between 100 mT and 1.70 T. We first calculate the macroscopic response of the
34 material in terms of induction profiles across the sheet thickness and classical loss $W_{\text{class}}(f)$, using the

35 electromagnetic diffusion equation and its solution. The calculation is performed by means of a simple
 36 numerical model, lumping in the normal magnetization curve the constitutive equation of the material.
 37 This permits us to separately determine the frequency dependent hysteresis $W_{\text{hyst}}(f)$ and excess $W_{\text{exc}}(f)$
 38 loss components and their evolution under increasing skin effect. Such evolution is measured against
 39 the direct findings on the dw dynamics provided by stroboscopic Kerr observations. These consistently
 40 show how the dw bowing, accommodating for deepening induction profile with frequency at low
 41 inductions, makes way for symmetrical reversal fronts, propagating from the sheet surface towards
 42 mid-plane, at high inductions.

43 **II. A classical model for the skin effect and losses**

44 *A. The induction profile*

45 The eddy currents circulating in a lamination under steady dynamic excitation are assumed to
 46 form a macroscopic pattern, investing the whole cross-sectional area, and localized patterns,
 47 surrounding the moving dws. The macroscopic currents are the result of the diffusion and superposition
 48 of the localized eddies and concentrate towards the sheet surface. The ensuing counterfield, combining
 49 with the uniform applied field, does impose, at any instant of time, a definite macroscopic profile $J(x)$
 50 to the magnetization across the sheet thickness, with obvious fluctuations at the scale of the domains.
 51 These will rearrange and adjust by the motion of the dws to such a profile. While the evolution of $J(x)$
 52 versus time, responsible for the homogeneous response of the material, is associated with $W_{\text{class}}(f)$, the
 53 superimposed fluctuations, with their localized currents, give rise to the extra dynamic contribution
 54 $W_{\text{exc}}(f)$. Let us then express the relationship between macroscopic magnetic induction $b(x,t)$ and
 55 magnetic field $h(x,t)$ at any frequency and peak induction value as a function of the spatial coordinate
 56 x across the sheet thickness d ($-d/2 \leq x \leq d/2$) according to the classical treatment by the Maxwell's
 57 diffusion equation

$$58 \quad \frac{\partial^2 h}{\partial x^2} - \sigma \frac{\partial b}{\partial t} = 0 \quad , \quad (1)$$

59 with the boundary conditions at mid-plane and surface

$$60 \quad \frac{\partial h}{\partial x} \Big|_{x=0} = 0 \quad , \quad \frac{\partial h}{\partial x} \Big|_{x=\pm d/2} = \sigma \frac{d}{2} \frac{dB}{dt} \quad (2)$$

61 where σ is the conductivity and $B(t)$ is the instantaneous induction of peak value B_p averaged over the
 62 sheet thickness.

63 To actual constitutive relation $b(h)$ is hysteretic in nature and its use in (1) would require a
 64 cumbersome numerical procedure.^{10, 11} To simplify the matter, we identify here the magnetic
 65 constitutive law with the normal magnetization curve. Equation **Erreur ! Source du renvoi**
 66 **introuvable.** is then solved by standard finite elements calculations, using the fixed point method.^{10, 11}
 67 The sheet thickness is subdivided in 100 layers and the macroscopic profile $J(x, t)$ of the polarization
 68 is calculated at any instant of time, for any measured J_p value, at the measuring frequencies. Fig. 1
 69 provides an example of the classically predicted behavior of the local peak polarization $J_p(x)$ across
 70 the sheet thickness at low inductions (average $J_p = 0.25$ T). Lack of flux penetration can be appreciated

71 in this case on increasing the frequency beyond about 200 Hz. The sheet interior soon attains a state of
 72 near-zero magnetization upon further frequency increase and at 10 kHz the magnetization change is
 73 predicted to occur within a $\sim 50 \mu\text{m}$ thick surface layer. With higher (thickness averaged) J_p values,
 74 however, the magnetization tends to approach the saturated state at the surface and the predicted $J_p(x)$
 75 profile takes a sharper shape (see inset in Fig. 1). At $f = 10 \text{ kHz}$ and $J_p = 1.0 \text{ T}$, a neat separation is, for
 76 example, seen to occur across the sheet thickness between an outer active region and an inner dead
 77 core. At very high inductions we eventually fall in the classical problem of magnetization reversal in a
 78 highly nonlinear material.¹⁴⁻¹⁷ Fig. 2, concerning the classical eddy current calculation at $f = 10 \text{ kHz}$
 79 and $J_p = 1.7 \text{ T}$, shows how reversal fronts are created and predicted to symmetrically proceed from the
 80 opposite sheet surfaces towards the sheet mid-plane along any semi-cycle. It is also shown how the
 81 local $J_p(x)$ eventually suffers only a slight depression at $x = 0$, as imposed by the need to reach high J_p
 82 . The front wave phenomenon actually appears, in this case, to be a specifically high-frequency effect,
 83 at odds with the similar effect postulated to occur in highly homogeneous materials (e.g. fine-grained
 84 non-oriented alloys) also at low frequencies. Kerr observations at power frequencies show that, even
 85 when it is cycled between $\pm J_p$ values not far from saturation (e.g. $J_p/J_s = 0.91$), a GO sheet exhibits the
 86 typical mechanisms of nucleation and growth of longitudinal domains by 180° dw motion.¹⁸ The
 87 question appears then one of understanding the role of the dws across a broad range of frequencies and
 88 the way the magnetization process can eventually end into a near-classical behavior. The question then
 89 arises of the phenomenology of magnetic losses and the way it can be assessed. It is in any case
 90 immediate to obtain in all cases, via the solutions of (1) and use of the Poynting theorem, or,
 91 equivalently, the integration of the square of the current density on the sheet thickness, the classical
 92 loss component $W_{\text{class}}(J_p, f)$.

94 III. Experimental method

95 A 0.29 mm thick high-permeability Fe-Si GO alloy (M2H type) was subjected to static and dynamic
 96 characterization up to 10 kHz. The measurements were performed on 300 mm long Epstein strips under
 97 controlled sinusoidal induction waveform, making use of a calibrated hysteresisgraph-wattmeter.¹⁹
 98 Two different magnetizer configurations were adopted. First, an appropriate number of strips was
 99 tested by the conventional Epstein frames, according to the standards IEC 60404-2 and IEC 60404-10.
 100 By this method, the lowest J_p values (100 mT and 250 mT) could be covered till 10 kHz. In order to
 101 deal with manageable signals, the upper J_p - f right corner was investigated by a single-strip tester, where
 102 the longitudinal GO strip, surrounded by a single layer magnetizing solenoid, is inserted between the
 103 pole faces of a laminated double-C yoke. A few-turn secondary coil is tightly wound at the strip centre
 104 and an H -coil is placed on top of it. The turns of the windings are all properly spaced, in order to avoid
 105 capacitive effects in the kilohertz range and single shot measurements guarantee negligible sample
 106 heating. A detailed description of this setup is provided in Ref..²⁰ A sufficiently wide overlapping $J_p -$
 107 f region could be covered with both Epstein frame and single-strip H -coil method, within $\pm 2 \%$

108 agreement between the respective loss figures. The full DC normal magnetization curve was obtained
109 by a point-by-point method.

110 Dynamic Kerr observations were carried out by means of stroboscopic imaging. The
111 magneto-optical setup employs an X-Cite series 120 lamp whose light is filtered, polarized and detected
112 by a gated intensified charge-coupled device (CCD) camera (Picostar LaVision). This permits one to
113 acquire equally time-spaced images at given frequency along the magnetization loop. The acquisition
114 is triggered by a signal with an adjustable phase with respect to the signal that drives the magnetization
115 of the sample. The signals are controlled by an Agilent 33522A function generator and visualized by
116 means of a LeCroy 816Zi oscilloscope. The magnetization of the sample, which is subjected to a tensile
117 stress of 9 MPa, is guaranteed by a split solenoid powered by a NF HSA4052 DC to 500kHz bipolar
118 amplifier. The sample induction is detected by means of a 3-turn pickup coil, wound close to the
119 investigated specularly polished area. Each magneto-optical image (resolution 0.5 $\mu\text{m}/\text{pix}$), detected
120 on a 5 mm diameter spot, is the average of 9000 frames, from which the usual background subtraction
121 subtraction is made. The sample temperature, monitored by a Pt100 resistance thermometer, was
122 allowed to rise during acquisition by a maximum of 15 $^{\circ}\text{C}$.

123

124 **III. Magnetic losses, domains wall dynamics, and their frequency evolution**

125

126 Whatever the frequency range, the domain structure, and the skin depth, the energy loss
127 decomposition method invariably applies to the analysis of the magnetic losses. It requires, as a first
128 step, the calculation of the classical loss component. As the $J_p(x)$ profiles in Fig. 1 suggest, the standard
129 analytical formula $W_{\text{class}} = \left(\frac{\pi^2}{6}\right)\sigma d^2 J_p^2 f$, requiring uniform induction, does not apply in these GO
130 sheets above a few hundred Hz. We are therefore obliged to resort to more complex approaches, like
131 the one discussed in the previous section. Relying then on the abovementioned calculations, we can
132 proceed to the broadband loss decomposition, examples of which are shown in Fig. 3a and 3b. These
133 refer to low ($J_p = 0.25$ T) and high ($J_p = 1.70$ T) induction values, respectively. It is apparent in these
134 figures that, with the emergence of the skin effect, the paths followed by W_{hyst} , W_{class} , and W_{exc} at high
135 frequencies are quite different at low and high inductions. In particular, W_{exc} and W_{class} dominate for J_p
136 $= 0.25$ T and $J_p = 1.70$ T, respectively, while the increase of W_{hyst} , while relevant at the lowest
137 inductions, always plays a minor role.

138 The starting point for the loss analysis is the previously discussed calculation of W_{class} , as
139 derived, together with the $J_p(x)$ profile, from the diffusion equation (1). It is apparent, looking at the
140 profiles, that W_{hyst} will increase together with $J_p(x)$ on going from the sheet core to the surface. At low
141 frequencies, where the skin effect is not an issue, the hysteresis loss $W_h(J_p)$ is frequency independent,
142 and can be obtained according to a straightforward extrapolation of the measured loss to zero
143 frequency.²¹ On the other hand, the present experiments show that a power law $W_{\text{hyst}} = kJ_p^\alpha$ for the
144 dependence of W_{hyst} on J_p applies, with $k = 14.15$ and $\alpha = 1.85$ up to $J_p = 1.5$ T and $k = 15.6$ and $\alpha =$

145 2.95 at higher J_p values (loss units in J/m^3). By taking into account that the quasi-static loss W_{hyst} is
 146 generated by very localized dissipative dw processes (Barkhausen jumps), we can easily retrieve its
 147 contribution at any frequency and average J_p value by integrating the local W_{hyst} along the $J_p(x)$ profile
 148

$$149 \quad W_{\text{hyst}}(J_p, f) = \frac{1}{d} \int_{-d/2}^{d/2} k J_p^\alpha(x) dx. \quad (2)$$

150

151 Once $W_{\text{class}}(f)$ and $W_{\text{hyst}}(f)$ are calculated, the excess loss component $W_{\text{exc}}(f) = W(f) - W_{\text{hyst}}(f) - W_{\text{class}}(f)$,
 152 where $W(f)$ is the measured energy loss, is obtained at all J_p values.

153 Looking at the examples shown in Fig. 3, one can see how the prediction of the statistical
 154 theory of losses, where, for given J_p , W_{hyst} is constant, $W_{\text{class}}(f)$ is, as previously recalled, a linear
 155 function of f , and $W_{\text{exc}}(f)$ is analytically formulated via defined statistical parameters,²² does not fully
 156 apply beyond about 200 Hz. It is observed, in particular, how the theoretical $W_{\text{exc}}(f)$ (STL line), deviates
 157 from the obtained $W_{\text{exc}}(f)$. It is observed as well that such a deviation reflects, on going to the kHz
 158 range, an important role of the dw processes at low inductions and a decreasing one at high inductions.
 159 We find, in particular, that about 70 % of the measured loss $W(f)$ is contributed by $W_{\text{exc}}(f)$ at 10 kHz
 160 and $J_p = 0.25$ T, while for $J_p = 1.70$ T, 95 % of it is covered at the same frequency by $W_{\text{class}}(f)$. To note
 161 also how the curve $W_{\text{class}}(f)$ at $J_p = 0.25$ T versus suffers predictable slope changes with increasing the
 162 frequency, in qualitative agreement with the corresponding behavior of the permeability at the sheet
 163 surface $\mu_{r,\text{surf}}$.

164 Supporting information regarding the evolution of the magnetization process versus f and J_p
 165 can be gained looking directly at the dw dynamics by the stroboscopic Kerr experiments. We provide
 166 in Figs. 4 and 5 few images taken on a well oriented [001](110) grain at low and high inductions and
 167 different frequencies. Fig. 4 shows an example of domain structure observed along a semi-cycle taken
 168 between $J_p = \pm 0.50$ T at 500 Hz and 10 kHz. A regular oscillatory motion of the walls, including
 169 bowing, is observed at 500 Hz. But at 10 kHz, near complete disappearance of the dws at the surface
 170 takes place, following multiplication and strong bowing. The antiparallel 180° dw structure is
 171 preserved and reappears in full, with denser population with respect the previous case, on the return
 172 from J_p . We conclude that at sufficiently low induction the magnetization reversal occurs at high
 173 frequencies by dw motion and bowing, consistent with the persisting large contribution of $W_{\text{exc}}(f)$ to
 174 the measured loss $W(f)$. Quite a different picture emerges in Fig. 5 from the Kerr sequence at 5 kHz
 175 taken along the semi-cycle with $J_p = \pm 1.70$ T. Starting from the fully saturated surface state observed
 176 at $J = J_p$, oppositely directed domains nucleate and grow at the surface, to eventually form a full reverse
 177 layer well before attaining the demagnetized state. This process, symmetrically occurring on the
 178 opposite sheet side, will expectedly proceed by a mechanism close to the front reversal motion
 179 predicted by the classical model, as sketched in Fig. 2. If this is the case, little loss contribution to the
 180 measured $W(f)$ is expected to come from the moving dws, as demonstrated by the faint proportion of
 181 $W_{\text{exc}}(f)$ predicted in Fig. 3b. This conclusion is further substantiated by the comparisons made between

182 the measured and the classically predicted hysteresis loops, when obtained in the upper J_p - f right
183 corner. We see in Fig. 6 how at 10 kHz and $J_p = 1.7$ T the loop computed via Eq. (1) and the measured
184 one have remarkably close shape and area. The slightly higher area of the experimental loop accounts
185 for residual contribution by the dw motion, in agreement with the high-frequency loss behaviour shown
186 in Fig. 3b. The slightly re-entrant shape of the experimental loop is related to the threshold field
187 required, as shown in Fig. 6, to start the nucleation of the surface domains. It is finally noted the close
188 similarity with the hysteresis loop (dashed line) calculated for an ideal step-like constitutive equation.¹⁶
189

190 **IV. Conclusions**

Magnetic losses have been investigated in grain-oriented high-permeability 0.29 mm thick Fe-Si sheet upon a wide range of peak polarization values ($100 \text{ mT} \leq J_p \leq 1.7 \text{ T}$) and frequencies (DC – 10 kHz). The loss properties have been assessed in the framework of the loss separation concept, generalized to cover the skin effect phenomena in the high-frequency region. We aim in this way to retrieve physical information on the broadband magnetization process in materials nowadays exposed to widening applicative areas, while overcoming the limitations of the empirical-phenomenological approaches proposed in the available literature. Looking for a manageable numerical treatment, the actual hysteretic magnetic constitutive equation is approximated with the normal magnetization curve, which is inserted in the Maxwell's diffusion equation. This is solved by a simple finite element algorithm. The macroscopic induction profiles versus sheet thickness as a function of J_p and f and the related classical energy loss component are thereby calculated. The familiar phenomenon of propagation of magnetization reversal fronts from the sheet surface to the mid-plane occurring along a semi-cycle is, in particular, retrieved in the upper J_p - f right corner. With the induction profile and the classical energy loss component W_{class} available over the whole frequency range, it is a simple matter to calculate the hysteresis W_{hyst} and the excess W_{exc} loss components, that is, to evaluate the evolution of the domain wall processes across the J_p - f matrix. In addition, we substantiate the related information by direct Kerr observations of the domain wall dynamics. We obtain that $W_{\text{dw}} = W_{\text{exc}} + W_{\text{hyst}}$ prevail at all frequencies over W_{class} at the lowest induction values, where the localized eddy currents are the major source of energy dissipation for moderate dw displacements and bowing. The macroscopic eddy current patterns, responsible for W_{class} , dominate instead upon increasing J_p at the highest frequencies, the higher J_p the broader the frequency range where this occurs. In the limit of high peak polarizations (e.g. $J_p = 1.7 \text{ T}$), the oscillatory motion of the 180° dw transforms, on attaining the kHz range, into a through propagation of magnetization reversals. Consequently, W_{dw} becomes negligible and the classical approach is sufficient for a reasonably accurate prediction of the measured losses.

- 193 ¹P. Siano, *Renewable and Sustainable Energy Rev.* **30**, 461 (2014).
194
195 ²H. Ichou, D. Roger, M. Rossi, T. Belgrand, and R. Lemaître, *J. Magn. Magn. Mater.* **504**, 166658 (230120).
196
197 ³M. A. Shamsuddin, F. Rojas, R. Cardenas, J. Pereda, M. Diaz, and R. Kennel, *Energies* **13**, 2319 (2020).
198
199 ⁴T. Belgrand, R. Lemaître, A. Benabou, J. Blaszowski et C. Wang, *AIP Advances* **8**, 047611 (2018).
200
201 ⁵G. Parent, R. Penin, J. P. Lecointe, J. F. Brudny, and T. Belgrand, *IEEE Trans. Magn.* **49**, 1977 (2013).
202
203 ⁶L. Gao, L. Zeng, J. Yang, and R. Pei, *AIP Advances* **10**, 015127 (2020).
204
205 ⁷K. Foster, F.E. Werner, and R.M. Del Vecchio, *J. Appl. Phys.* **53**, 8308 (1982).
206
207 ⁸R. Liu and L. Li, *IEEE Trans- Pow. Electr.* **36**, 2009 (2020).
208
209 ⁹J. Mühlethaler, J. Biela, J. W. Kolar, and A. Ecklebe, *IEEE Trans. Pow. Electr.* **27**, 953 (2012).
210
211 ¹⁰C. Appino, G. Bertotti, D. Binesti, O. Bottauscio, M. Chiampi, J.P. Ducreux, F. Fiorillo, M. Repetto, and P.
212 Tiberto, *J. Appl. Phys.* **79**, 4575 (1996).
213
214 ¹¹L. Dupre, O. Bottauscio, M. Chiampi, M. Repetto, and J. Melkebeek, *IEEE Trans. Magn.* **35**, 4171 (1999).
215
216 ¹²C. Beatrice, C. Appino, O. de la Barrière, F. Fiorillo, and C. Ragusa, *IEEE Trans. Magn* **50**, 6300504 (2014).
217
218 ¹³S.E. Zirka, Y.I. Moroz, S. Steentjes, K. Hameyer, K. Chwastek, S. Zurek, and R.G. Harrison, *J. Magn. Magn.*
219 *Mater.* **394**, 229 (2015).
220
221 ¹⁴S. E. Zirka, Y. I. Moroz, P. Marketos, A. J. Moses, D. C. Jiles, and T. Matsuo, *IEEE Trans. Magn.* **44**, 2113
222 (2008).
223
224 ¹⁵C. Serpico, C. Visone, I. D. Mayergoyz, V. Basso, and G. Miano, *J. Appl. Phys.* **87**,. 6923 (2000).
225
226 ¹⁶G. Bertotti, *Hysteresis in Magnetism*, Academic Press, San Diego, CA (1998) p. 407.
227
228 ¹⁷F. Friedlaender, *Trans. AIEE, Part I* **75**, 268(1956).
229
230 ¹⁸R. Schaefer, I. Soldatov, and S. Arai, *J. Magn. Magn. Mater.* **474**, 221 (2019).
231
232 ¹⁹F. Fiorillo, *Measurement and Characterization of Magnetic Materials*, (Academic-Elsevier, San Diego CA,
233 2004) p. 362.
234
235 ²⁰O. de la Barriere, C. Ragusa, M. Khan, C. Appino, F. Fiorillo, and F. Mazaleyrat, *IEEE Trans. Magn.* **52**,
236 2001204 (2016).
237
238 ²¹G. Bertotti, *IEEE Trans. Magn.* **24**, 621 (1988).
239
240 ²²E. Barbisio, F. Fiorillo, and C. Ragusa, *IEEE Trans. Magn.* **40** 1810 (2004).
241

243
 244
 245
 246
 247
 248
 249
 250
 251
 252
 253
 254
 255
 256
 257
 258
 259
 260
 261
 262
 263
 264
 265
 266

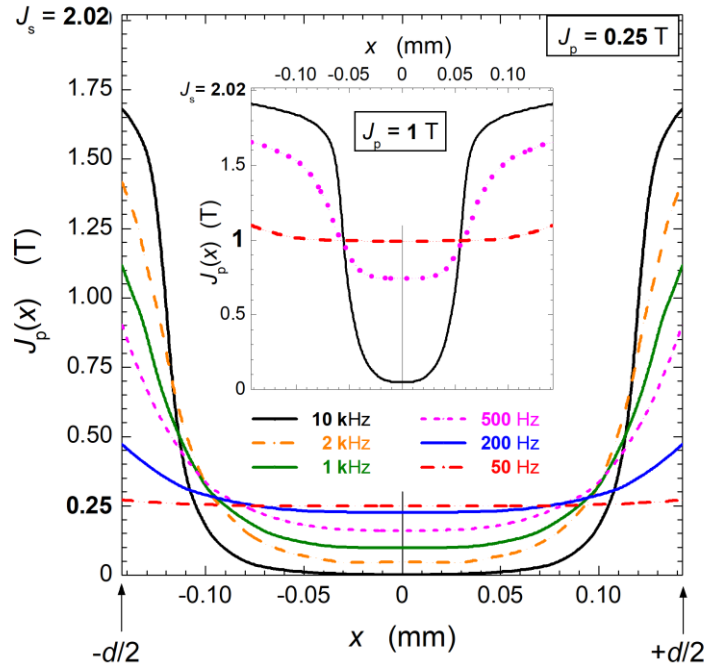


Fig. 1. Calculated profiles of the local peak polarization value $J_p(x)$ across the 0.29 mm thick GO sheet and their dependence on the magnetizing frequency for average peak polarization $J_p = 0.25$ T. The inset shows the evolution taken by such profiles for $J_p = 1.0$ T.

267
 268
 269
 270
 271
 272
 273
 274

275
 276
 277
 278
 279
 280
 281
 282
 283
 284
 285
 286
 287
 288
 289
 290
 291
 292

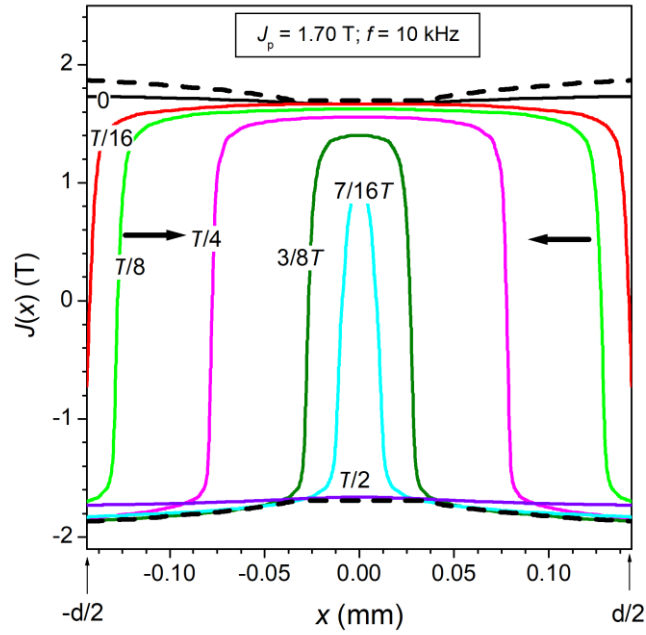


Fig. 2. Reversal fronts symmetrically proceeding inward from the opposite sheet surfaces at high frequencies and high induction values, as predicted to occur by the classical approach in the 0.29 mm GO sheet. The calculations assume a constitutive equation coincident with the normal magnetization curve. The fronts are shown at different instants of time ($T = 1/f$) along a semi-cycle taken at 10 kHz between $J_p = \pm 1.7$ T. The dashed lines shows the corresponding profile of the peak polarization values $\pm J_p(x)$.

293
 294
 295
 296
 297
 298
 299
 300
 301
 302
 303
 304
 305
 306
 307
 308
 309
 310
 311
 312
 313
 314
 315
 316
 317
 318

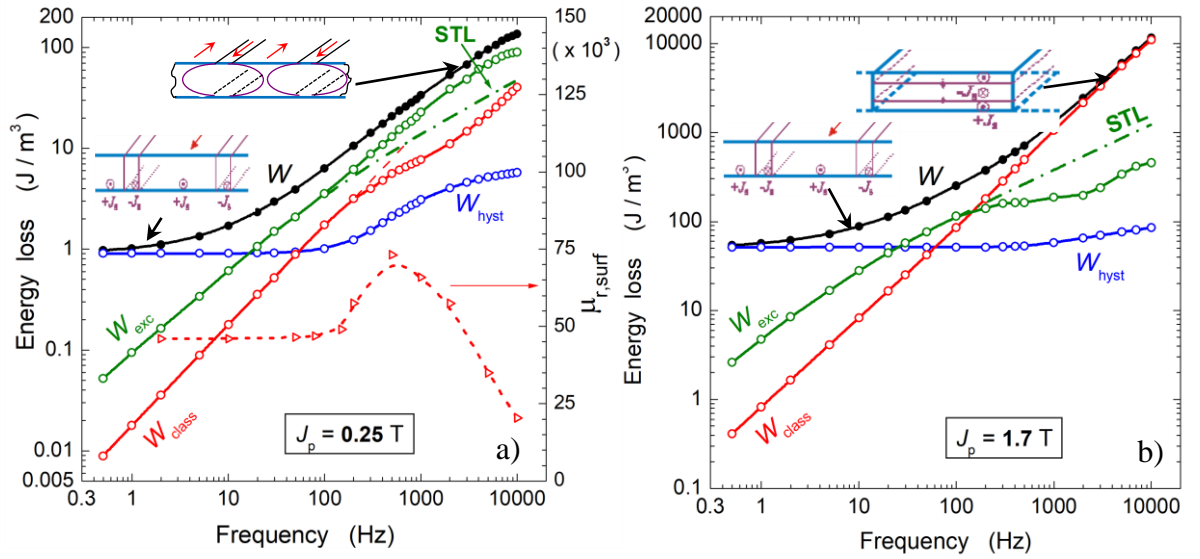


Fig. 3. DC-10 kHz loss decomposition in the 0.29 mm thick GO sheet at low and high inductions. Largely different behaviours of the loss components for $J_p = 0.25$ T and $J_p = 1.70$ T take place beyond a few hundred Hz, because of the emerging non-homogeneity of the induction across the sheet thickness. To note the behaviour of the permeability $\mu_{r,surf}$ at the sheet surface versus f , which correlates with the behaviour of W_{class} , and the prediction of W_{exc} by the statistical theory of losses (STL line), which deviates from the experimental result upon the establishment of the skin effect.

370
371
372
373
374
375
376
377
378
379
380
381
382
383
384
385
386
387
388
389
390
391
392
393
394
395
396
397
398
399
400
401
402
403
404
405
406
407
408
409
410
411
412
413
414
415
416
417
418
419
420

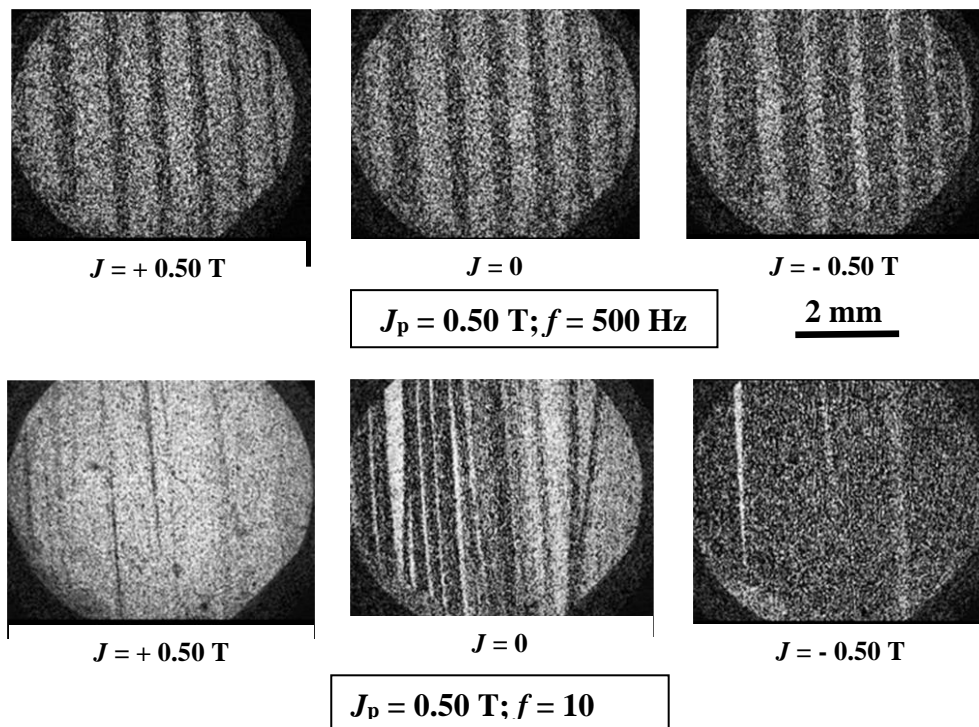


Fig. 4. Domain structure in a well oriented grain and its evolution along a semi-cycle between $\pm 0,50$ T at 500 Hz and 10 kHz.

421
422
423
424
425
426
427
428
429
430
431
432
433
434
435
436
437
438
439
440
441
442
443
444
445
446
447
448
449
450
451
452
453

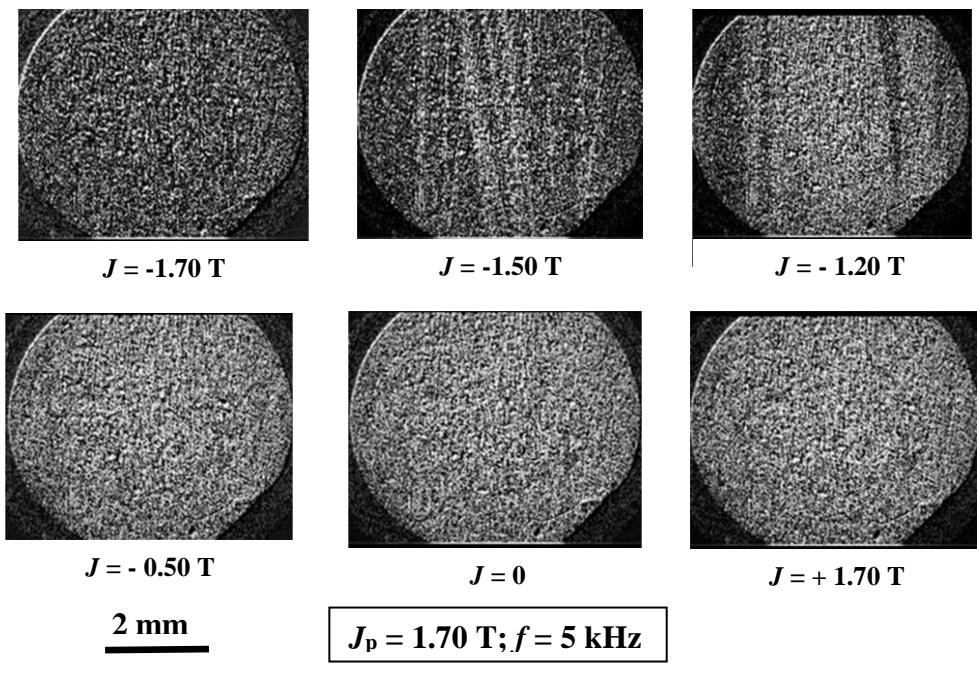


Fig.5. As in Fig. 4 along an ascending semi-cycle run between -1.70 T to +1.70 T at 5 kHz.

454
455
456
457
458
459
460
461
462
463
464
465
466
467
468
469
470

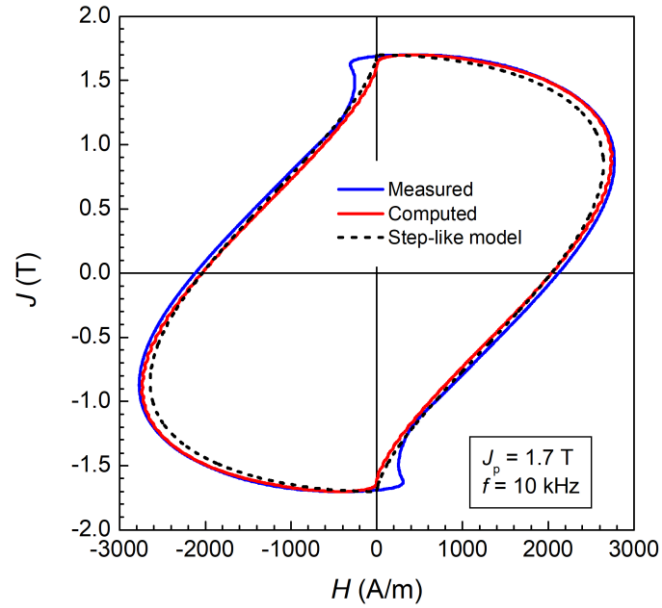


Fig. 6. The hysteresis loop classically computed via the diffusion Eq. (1) compares with the hysteresis loop measured at 10 kHz and $J_p = 1.70 \text{ T}$, in good agreement with a magnetization mechanism in the sheet by inward motion of reversal fronts, as sketched in Fig. 2. A faint contribution to dissipation by dw motion results in a slightly wider experimental loop. To note a threshold mechanism at the beyond the romance point, descending from the nucleation of surface domains, as revealed by the images of Fig. 5. The dashed line is calculated for the ideal case of a step-like constitutive equation ranging between $\pm 1.85 \text{ T}$.¹⁶